Non-unit Protection of Parallel Lines Connecting Solar Photovoltaic Plants

Arghadeep Chowdhury, Subhadeep Paladhi and Ashok Kumar Pradhan, *Senior Member, IEEE*

***Abstract*—Fault current control by solar plant converters introduces different fault characteristics compared to conventional synchronous generator based systems resulting in numerous issues to the available protection methods. In this paper, the issues with conventional distance relaying is analyzed while protecting parallel lines connecting solar plant to grid and a new protection method is proposed using local voltage and current data. The proposed non-unit protection method derives positive sequence reactive powers for both lines for different solar plant operating conditions and uses their difference to ensure correct zone-1 protection. For faults during single circuit operation, the method includes an additional scheme comprising of instantaneous zero-sequence overcurrent check and delayed distance relaying to derive correct protection decision. Performance of the proposed non-unit protection method is tested for parallel lines connecting solar plant in a 39-bus test system for different situations using PSCAD/EMTDC simulated data and found to be accurate. Comparative assessment reveals the high reliability of the proposed method.**

***Index Terms*—Solar photovoltaic plant, parallel lines, power system faults, distance relaying, Non-unit protection.**

I. Introduction

A. Motivation and Incitement

NOWADAYS the integration of large scale solar photovoltaic (PV) plants to the high voltage transmission network is increasing rapidly to mitigate the environmental degradation and energy demand [1], [2]. The PV plants when connected to the grid with parallel lines enhance system reliability. Fault ride through (FRT) operation and different control schemes adopted in the converters associated with the renewable plants modulate the voltage and current waveforms significantly during fault [3]. With such a change in the fault behavior, available protection schemes for parallel lines are under scrutiny.

B. Literature review

Available line protection techniques are categorized in this section to highlight their applicability and limitations for protection of parallel lines connecting solar PV plants.

1) Distance relay based approaches: Performance of distance relay, widely used as the non-unit protection scheme for transmission lines, is affected by the mutual coupling associated with parallel line configuration [4]. Different impedance based algorithms are available for compensating the mutual coupling effect [5]–[9], which assume both side source impedances to be homogeneous with the line impedance. This is not true for a system integrating converter interfaced renewable plants (CIRPs). Communication assisted schemes, available in [10], [11] to overcome the mutual coupling effect in parallel-line configuration, cannot decide in case of communication failure.

2) Cross-differential algorithms: Cross differential relaying (CDR) compares the local end current magnitudes in both lines in a parallel-line configuration to identify the faulted line [4], [12], [13]. The CDR principle does not consider the non-homogeneity in case of a power system with CIRPs. Significant phase angle difference observed between both end fault currents in a parallel line configuration in the presence of CIRPs may result in CDR maloperation at times.

3) Protection schemes with CIRPs: Different distance protection schemes are available in [14]–[16] for lines emanating from CIRPs. An adaptive distance relaying scheme is proposed in [14] for single line connecting PV plant. The method computes the faulted path current angle by applying a simplified current distribution relation and derives correct decision. Such simplification is not acceptable for parallel lines, especially when the grid becomes weaker or lines become longer. Correct performance of distance relay in a solar PV integrated network is ensured in [15] by modifying the control scheme of PV plants. Such modification imitating synchronous generator fault characteristic is difficult to generalize with different control operations in PV plants. A delayed distance protection is recommended in [16] for PV side distance relays to eliminate the infeed effect by instantaneous remote end breaker operation. Such a delay may cause unintentional triggering of the remote end relays protecting the healthy lines in a parallel line configuration and also affect the system stability.

4) Other available approaches: A reactive power based method, available in [17], can protect parallel lines only for ungrounded faults. The modal current based approach available in [18] for parallel line protection requires reliable communication channel for its operation.

C. Contribution

In this work, the performance of distance relay protecting parallel lines connecting PV plants to the grid is analyzed and found to have limitations for Zone-1 faults. A local data based non-unit protection method is proposed for such line configurations using positive sequence reactive power difference. The main contributions of this paper are summarized below.

1) Fault current distribution in parallel lines and their relations with the corresponding voltage component are derived for different operating conditions of the solar plant (connected at one end) using a generalized sequence network, applicable for all types of faults.
2) Positive sequence reactive powers are computed for both lines using local end positive sequence voltage and corresponding current components. Their difference is applied for identifying Zone-1 faults in such line configurations.

Arghadeep Chowdhury and Ashok Kumar Pradhan are with the Department of Electrical Engineering, Indian Institute of Technology, Kharagpur 721302, India (e-mail: argha8900397358.2012@gmail.com; pradhan.ashok@gmail.com). Subhadeep Paladhi is with the Department of Electronic and Electrical Engineering, University of Strathclyde, G11XQ Glasgow, U.K. (e-mail: paladhisubha91@gmail.com).

This is a peer-reviewed, accepted author manuscript of the following article: Chowdhury, A., Paladhi, S., & Pradhan, A. K. (2022). Non-unit protection of parallel lines connecting solar photovoltaic plants. IEEE Systems Journal, 1-10. https://doi.org/10.1109/JSYST.2022.3229349

3) An additional scheme comprising of instantaneous zero-sequence overcurrent check and delayed distance relaying is included to derive correct protection decision for faults during single circuit operation.

Performance of the proposed method is tested for PV integrated modified 39-bus New England system, a 9-bus system with 100% PV penetration and an existing solar park integrated parallel-line based Indian power grid network using PSCAD/ EMTDC simulated data for different types of faults with variation in fault resistance, location, power flow condition, connected renewable source type and associated grid code. The performance is also tested for cross-country faults, in the presence of inter-harmonics and during power swing. Comparative assessment is provided to highlight the high reliability of the proposed non-unit protection method. .

II. System Description

A double circuit line connecting a solar plant to the grid is shown in Fig.1. The plant consists of multiple photovoltaic units with each one connected to the collector bus through a DC/AC inverter operating in grid following mode and a step-up transformer. The inverters interfacing each unit is controlled in synchronous reference frame with feedforward compensation [19] and inject balanced current into the grid even for asymmetrical faults satisfying reactive current requirement followed by the grid code mentioned in [15]. The solar plant being connected to the bulk-power system consider internal protection guidelines same as in the NERC reliability standard [20]. Both the lines (line-1 and line-2) are protected by distance relays. Relays at the PV end are shown in Fig. 1, which use bus voltage and corresponding line currents ($I_M^{(1)}$ and $I_M^{(2)}$) at M. Superscripts '1' and '2' indicate measurements for line-1 and line-2 respectively. System parameters are provided in Appendix-II.

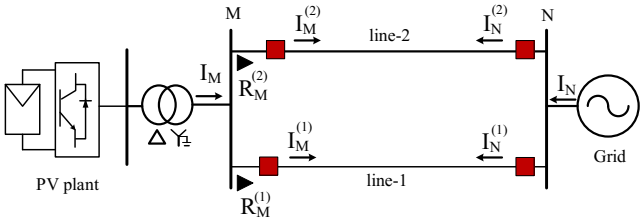

Fig. 1. Parallel lines connecting a PV plant to the grid.

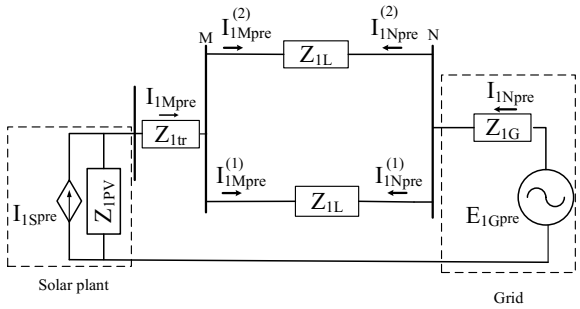

Fig. 2. Equivalent model of the system in Fig.1 during prefault.

Figure 2 shows the equivalent positive sequence model of the system in Fig.1 during prefault condition. Both the transmission lines are considered to be homogeneous with a positive sequence impedance, Z_{1L}. The Thevenin's equivalent of the grid is represented using a voltage source (E_{1Gpre}) with an internal impedance (Z_{1G}) in series. The grid following converter connecting solar plant is represented with a dependent current source (I_{1Spre}) in parallel with a high impedance (Z_{1PV}) [21]. The solar plant is connected to bus M with the positive sequence transformer impedance Z_{1tr}. Subscript '1' represents the positive sequence component.

III. Problem Statement

Figure 3 shows the generalized sequence network of the system in Fig. 1 for a fault in line-1 at a distance of x pu from bus M. Z_F is the total faulted path impedance consisting of equivalent negative sequence impedance (Z_2^{eq}), equivalent zero sequence impedance (Z_0^{eq}) and fault resistance (R_F). Z_F for different types of faults are expressed in (1).

$$\begin{aligned} Z_F &= Z_2^{eq} + (Z_0^{eq} + 3R_F);\ \text{for line-to-ground faults} \\ Z_F &= Z_2^{eq} + R_F;\ \text{for line-to-line faults} \\ Z_F &= Z_2^{eq} || (Z_0^{eq} + 3R_F);\ \text{for double line-to-ground faults} \\ Z_F &= R_F;\ \text{for 3-phase ground faults} \end{aligned} \tag{1}$$

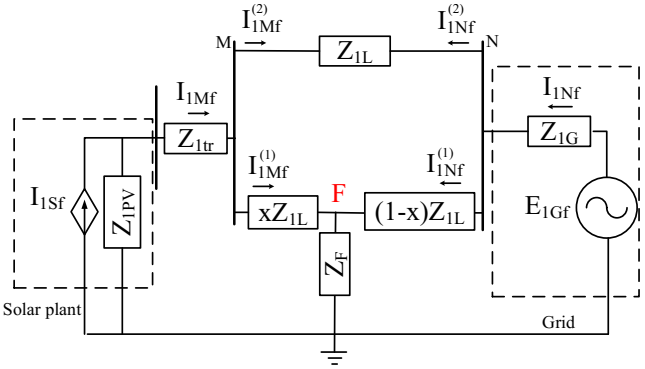

Fig. 3. Sequence network of the system in Fig. 1 for a fault in line-1.

Apparent impedance ($Z_M^{(1)}$) calculated by the distance relay $R_M^{(1)}$ (as shown in Fig. 1) for such a situation is given by

$$\begin{aligned} Z_M^{(1)} = \frac{V_{rM}}{I_{rM}^{(1)}} &= xZ_{1L} + R_F\left(\frac{I_F^{(1)}}{I_{rM}^{(1)}}\right) \\ &= Z_{MF}^{(1)} + \Delta Z. \end{aligned} \tag{2}$$

where V_{rM} and $I_{rM}^{(1)}$ are operating voltage and current for the relay $R_M^{(1)}$. $I_F^{(1)}$ is the faulted path current [14]. It is observed from (2) that the impedance calculated by the relay includes an additional impedance (ΔZ) with the faulted section impedance ($Z_{MF}^{(1)} = xZ_{1L}$) and can be expressed as in (3).

$$\Delta Z = R_F\left(\frac{I_F^{(1)}}{I_{rM}^{(1)}}\right) = R_F\left(1 + \frac{I_{rN}^{(1)}}{I_{rM}^{(1)}}\right) \tag{3}$$

The current ratio varies significantly due to the limited and modulated fault current from the solar plant and results in maloperation for the distance relay. In addition, the presence of zero-sequence mutual impedance in parallel line configuration amplifies the issue further [4].

Limited performance of the distance relay for such a line configuration is demonstrated in the system of Fig.1 where the PV plant is of 300 MW capacity. BCG faults are created in line-1 at a distance of 0.7 pu from bus M with $R_F = 10\ \Omega$, while the PV plant is complied with a dynamic reactive current characteristics as in [15] and the generation is varied

from 100 to 300 MW. For BCG fault, $I_{rM}^{(1)}$ and $I_{rN}^{(1)}$ in (3) are substituted with $(I_{BMf}^{(1)} - I_{CMf}^{(1)})$ and $(I_{BNf}^{(1)} - I_{CNf}^{(1)})$ respectively [14]. A significant difference in magnitude of $(I_{BNf}^{(1)} - I_{CNf}^{(1)})$ and $(I_{BMf}^{(1)} - I_{CMf}^{(1)})$ can be observed from the results shown in Fig.4 (a). In addition, the results shown in Fig.4(b) demonstrate the phase difference. This leads to a high value of ΔZ to be present in the apparent impedance $(Z_M^{(1)})$ calculated by the PV side distance relay $(R_M^{(1)})$ and results in an underreach situation for the relay set with a quadrilateral characteristic [22], as shown in 5. It is noticed that the calculated apparent impedances are much higher when the solar plant generates lesser power than the rated capacity, increasing the chance of distance relay maloperation.

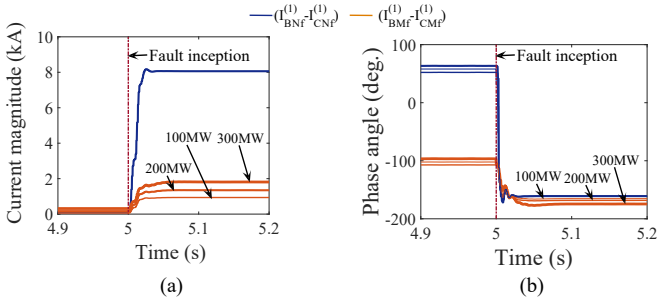

Fig. 4. (a) Magnitudes and (b) phase angles of $\left(I_{BMf}^{(1)} - I_{CMf}^{(1)}\right)$ and $\left(I_{BNf}^{(1)} - I_{CNf}^{(1)}\right)$ for BCG fault created in line-1 of the system in Fig. 1 for different PV plant capacity.

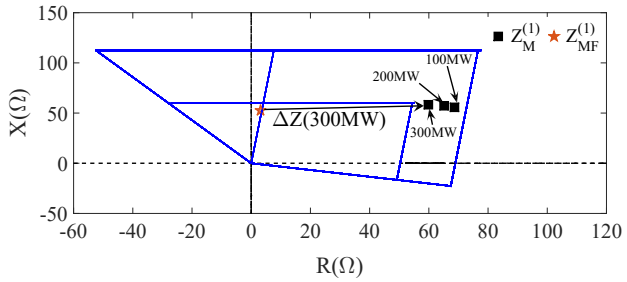

Fig. 5. Underreach performance of distance relay for fault in parallel line connected with PV plant of different capacity.

IV. Proposed Method

In order to mitigate the issue associated with distance relay for Zone-1 faults in parallel lines connecting solar PV plant (as demonstrated in Section III), a local data based protection algorithm is proposed in this section.

A. Identification of Zone-1 fault in parallel lines

Applying current distribution property in Fig.3 for a fault in line-1, positive sequence currents at terminal M can be expressed as,

$$\begin{aligned} I_{1Mf}^{(1)} &= I_{1Sf}S_1 + I_{1Nf}S_2 \\ I_{1Mf}^{(2)} &= I_{1Sf}(1-S_1) - I_{1Nf}S_2. \end{aligned} \tag{4}$$

where, I_{1Sf} and I_{1Nf} are the positive sequence current from the solar plant and grid side during fault. S_1 and S_2 are expressed in (5).

$$\begin{aligned} S_1 &= \frac{(1-x)Z_{1L}+Z_{1G}(2-x)+Z_F}{Z_{1L}(1-x^2)+2Z_{1G}+2Z_F} \\ S_2 &= \frac{(1-x)}{2} \end{aligned} \tag{5}$$

Using sequence network, I_{1Nf} can be obtained as in (6).

$$I_{1Nf} = \frac{2E_{1Gf}}{Z_{1L}(1-x^2)+2Z_{1G}+2Z_F}. \tag{6}$$

A relation is derived in (7) from (4) by multiplying V_{1Mf} with the conjugate of $I_{1MF}^{(1)}$ and equating the imaginary terms of both sides.

$$\begin{aligned} |V_{1Mf}||I_{1Mf}^{(1)}|sin(\theta_{1vf}-\angle I_{1Mf}^{(1)}) &= |V_{1Mf}||I_{1Sf}||S_1|sin(\theta_f-\theta_{S_1}) \\ &+|V_{1Mf}||I_{1Nf}||S_2|sin(\theta_{1vf}-\theta_{1Nf}) \end{aligned} \tag{7}$$

θ_{1vf} and θ_{1Nf} in (7) are the phase angles of V_{1Mf} and I_{1Nf}. θ_f is the power factor angle at bus M, which varies between 0 to $\pi/2$ during fault depending on the grid code [23]. Thus, $I_{1Sf} = |I_{1Sf}|\angle(\theta_{1vf} - \theta_f)$. Similarly, another relation is derived in (8) from the expression of $I_{1MF}^{(2)}$ in (4).

$$\begin{aligned} |V_{1Mf}||I_{1Mf}^{(2)}|sin(\theta_{1vf}-\angle I_{1Mf}^{(2)}) &= |V_{1Mf}||I_{1Sf}||(S_1^{'})|sin(\theta_f-\theta_{S_1'}) \\ &-|V_{1Mf}||I_{1Nf}||S_2|sin(\theta_{1vf}-\theta_{1Nf}) \end{aligned} \tag{8}$$

where,

$$S_1^{'} = (1-S_1) = \frac{x((1-x)Z_{1L}+Z_{1G})+Z_F}{Z_{1L}(1-x^2)+2Z_{1G}+2Z_F} \tag{9}$$

Left hand side of (7) is the positive sequence reactive power $(Q_{1M}^{(1)})$ flowing through line-1, which is expressed separately in (10).

$$Q_{1M}^{(1)} = |I_{1Mf}^{(1)}||V_{1Mf}|sin(\theta_{1vf} - \angle I_{1Mf}^{(1)}) \tag{10}$$

Similarly, the positive sequence reactive power of line-2 $(Q_{1M}^{(2)})$ is obtained from (8) and expressed in (11).

$$Q_{1M}^{(2)} = |I_{1Mf}^{(2)}||V_{1Mf}|sin(\theta_{1vf} - \angle I_{1Mf}^{(2)}) \tag{11}$$

Difference in positive sequence reactive powers in both the lines (ΔQ_{1M}) is obtained in (12) by subtracting (8) from (7).

$$\begin{aligned} \Delta Q_{1M} &= Q_{1M}^{(1)} - Q_{1M}^{(2)} \\ &= |V_{1Mf}||I_{1Sf}|\left(|S_1|sin(\theta_f-\theta_{S_1})-|S_1^{'}|sin(\theta_f-\theta_{S_1'})\right) \\ &+2|V_{1Mf}||I_{1Nf}||S_2|sin(\theta_{1vf}-\theta_{1Nf}) \end{aligned} \tag{12}$$

The expression in (12) is further analysed separately for different power factor modes of operation of the PV plant.

1) During PV plant operation in zero power factor (zpf) mode: For zpf mode of operation, $\theta_f = \pi/2$. Following the substitution of θ_f, (12) is rewritten in (13).

$$\begin{aligned} \Delta Q_{1M} &= |V_{1Mf}||I_{1Sf}|\left(|S_1|cos(\theta_{S_1}) - |S_1^{'}|cos(\theta_{S_1'})\right) \\ &+2|V_{1Mf}||I_{1Nf}||S_2|sin(\theta_{1vf}^{zpf}-\theta_{1Nf}) \end{aligned} \tag{13}$$

ΔQ_{1M} in (13) is always greater than zero as $i)$ $|S_1|cos(\theta_{S_1}) > |S_1^{'}|cos(\theta_{S_1'})$ and $ii)$ $sin(\theta_{1vf}^{zpf}-\theta_{1Nf}) > 0$.

i). Proof of $|S_1|cos(\theta_{S_1}) > |S_1^{'}|cos(\theta_{S_1'})$*:* Neglecting the resistance of transmission line and grid impedances in (5) and (9), $cos(\theta_{S_1})$ and $cos(\theta_{S_1'})$ are expressed in (14).

$$cos(\theta_{S_1}) = \frac{1}{\sqrt{1+(P_1/P_2)^2}}, \quad cos(\theta_{S_1'}) = \frac{1}{\sqrt{1+(P_1/P_3)^2}} \tag{14}$$

P_1, P_2 and P_3 in (14) are expanded in (15), where X_{1L} and X_{1G} are the positive sequence reactances of line and grid. Z_F is divided into real (R_F^{eq}) and imaginary (X_F^{eq}) parts.

$$\begin{aligned} P_1 &= (1\text{–}x)(X_{1L}(1\text{-}x)+2X_{1G}) \\ P_2 &= 2R_F^{eq}+(x(1\text{–}x)X_{1L}+X_F^{eq})(X_{1L}(1\text{–}x^2)+2X_{1G}+2X_F^{eq}) \\ &\quad +(X_{1L}(1\text{–}x^2)+2X_{1G}+2X_F^{eq})((1\text{–}x)(X_{1L}+X_F^{eq})+(2\text{–}x)X_{1G}) \\ P_3 &= P_2\text{–}(X_{1L}(1\text{–}x^2)+2X_{1G}+2X_F^{eq})((1\text{–}x)(X_{1L}+X_F^{eq})+(2\text{–}x)X_{1G}) \end{aligned} \tag{15}$$

x being in the range of $[0, 1]$, P_2 in (15) is observed to be greater than P_3 and it results in $\frac{1}{\sqrt{1+(P_1/P_2)^2}} > \frac{1}{\sqrt{1+(P_1/P_3)^2}}$. This indicates $cos(\theta_{S_1})$ in (14) to be greater than $cos(\theta_{S_1'})$. In addition, $|(1\text{–}x)Z_{1L}+Z_{1G}(2\text{–}x)+Z_F|$ in (5) being greater than $|x((1\text{–}x)Z_{1L}+Z_{1G}) + Z_F|$ in (9), $|S_1|$ is found to be greater than $|S_1^{'}|$. Thus,

$$|S_1|cos(\theta_{S_1}) > |S_1^{'}|cos(\theta_{S_1'}) \tag{16}$$

ii). Proof of $sin(\theta_{1vf}^{zpf}\text{–}\theta_{1Nf}) > 0$: A relation is derived in (17) by substituting $\theta_f = \pi/2$ in the expression of θ_{1vf} (as provided in (38) in Appendix-I).

$$\theta_{1vf}^{zpf}\text{-}\theta_{1Nf} = sin^{-1}\left(\frac{|I_{1Sf}||X_{1L}||D_1|sin(\angle D_1)}{|E_{1Gf}||K_1|}\right) + \angle K_1\text{–}\theta_{1Nf} \tag{17}$$

(17) is simplified in (18) by eliminating $\angle D_1$ and $\angle K_1$, which are obtained as zero for 3-phase bolted faults (considering the homogeneity in transmission line and grid impedances in (39) in Appendix-I).

$$\theta_{1vf}^{zpf} - \theta_{1Nf} = -\theta_{1Nf} \tag{18}$$

From (6), θ_{1Nf} is obtained in the range of $(-\frac{\pi}{2}, 0)$. Thus, $sin(\theta_{1vf}^{zpf} - \theta_{1Nf})$ is positive for 3-phase faults. For asymmetrical faults with $\mathrm{R_F}$, (17) is simplified in (19) by neglecting grid and line resistances following the substitution of D_1, K_1 and θ_{1Nf} obtained from (39) (in Appendix-I) and (6).

$$\begin{aligned} \theta_{1vf}^{zpf}\text{–}\theta_{1Nf} = & sin^{-1}\left(\frac{|I_{1Sf}||X_{1L}||D_1|sin(\angle D_1)}{|E_{1Gf}||K_1|}\right) \\ & + tan^{-1}\left(\frac{x(1-x)X_{1L} + 2X_F^{eq}}{2R_F^{eq}}\right) \end{aligned} \tag{19}$$

From (39) it is observed that $|\frac{D_1}{K_1}| < 1$ as $|x(1-x)Z_{1L} + x(2-x)Z_{1G} + Z_F| < |x(1-x)Z_{1L} + 2Z_F|$. Further, the magnitude of E_{1Gf} becomes much higher than $|I_{1Sf}||X_{1L}|$ due to the limited magnitude of I_{1Sf} from the PV plant. Therefore, $\frac{|I_{1Sf}||X_{1L}||D_1|sin(\angle D_1)}{|E_{1Gf}||K_1|} << 1$ and a relation can be obtained as in (20).

$$sin^{-1}\left(\frac{|I_{1Sf}||X_{1L}||D_1|sin(\angle D_1)}{|E_{1Gf}||K_1|}\right) \approx 0 \tag{20}$$

Applying (20), (19) is simplified in (21).

$$\theta_{1vf}^{zpf}\text{–}\theta_{1Nf} = tan^{-1}\left(\frac{x(1-x)X_{1L} + 2X_F^{eq}}{2R_F^{eq}}\right) \tag{21}$$

X_{1L}, X_F^{eq} and R_F^{eq} in (21) being always positive, a relation is derived in (22), which is valid for all symmetrical and asymmetrical faults.

$$sin(\theta_{1vf}^{zpf} - \theta_{1Nf}) > 0 \tag{22}$$

Thus applying the relations obtained from (16) and (22) in (13), a condition is derived as in (23) for faults in line-1.

$$\Delta Q_{1M} > 0 \tag{23}$$

2) During PV plant operation in unity power factor (upf) mode: For upf mode of operation, $\theta_f = 0$. This is substituted in (12) and rewritten in (24).

$$\begin{aligned} \Delta Q_{1M} = & |V_{1Mf}||I_{1Sf}|\left(|S_1^{'}|sin(\theta_{S_1'}) - |S_1|sin(\theta_{S_1})\right) \\ & +2|V_{1Mf}||I_{1Nf}||S_2|sin(\theta_{1vf}^{upf}\text{–}\theta_{1Nf}) \end{aligned} \tag{24}$$

$sin(\theta_{S_1})$ and $sin(\theta_{S_1'})$ in (24) are expressed in (25) using P_1, P_2 and P_3 obtained from (15).

$$sin(\theta_{S_1}) = \frac{1}{\sqrt{1+(P_2/P_1)^2}}, \quad sin(\theta_{S_1'}) = \frac{-1}{\sqrt{1+(P_3/P_1)^2}} \tag{25}$$

Substituting $sin(\theta_{S_1})$, $sin(\theta_{S_1'})$ (obtained from (25)) and S_2 (obtained from (5)) in (24), a relation is derived in (26).

$$\begin{aligned} \Delta Q_{1M} = & |V_{1Mf}||I_{1Nf}||(1\text{–}x)|sin(\theta_{1vf}^{upf}\text{–}\theta_{1Nf}) \\ & -|V_{1Mf}||I_{1Sf}|\left(\frac{|S_1^{'}|}{\sqrt{1+(P_3/P_1)^2}} + \frac{|S_1|}{\sqrt{1+(P_2/P_1)^2}}\right) \end{aligned} \tag{26}$$

Substituting $\theta_f = 0$ in the expression of θ_{1vf} (as provided in (38) in Appendix-I), a relation is derived in (27).

$$\theta_{1vf}^{upf}\text{–}\theta_{1Nf} = sin^{-1}\left(\frac{|I_{1Sf}||X_{1L}||D_1|cos(\angle D_1)}{|E_{1Gf}||K_1|}\right) + \angle K_1\text{–}\theta_{1Nf} \tag{27}$$

The relation in (27) is simplified in (28) by neglecting grid and line resistances following the substitution of K_1 and θ_{1Nf} obtained from (39) (in Appendix-I) and (6) respectively.

$$\begin{aligned} \theta_{1vf}^{upf}\text{–}\theta_{1Nf} = & sin^{-1}\left(\frac{|I_{1Sf}||X_{1L}||D_1|cos(\angle D_1)}{|E_{1Gf}||K_1|}\right) \\ & + tan^{-1}\left(\frac{x(1-x)X_{1L} + 2X_F^{eq}}{2R_F^{eq}}\right) \end{aligned} \tag{28}$$

From (39) (as derived in Appendix-I), the range of $\angle D_1$ can be obtained as $(-\frac{\pi}{2}, 0)$. This results in $cos(\angle D_1)$ to be positive. With the relations $\frac{|I_{1Sf}||X_{1L}||D_1|sin(\angle D_1)}{|E_{1Gf}||K_1|} << 1$, and $tan^{-1}\left(\frac{x(1-x)X_{1L}+2X_F^{eq}}{2R_F^{eq}}\right) \leq \pi/2$ (as obtained earlier), the range of $(\theta_{1vf}^{upf}\text{–}\theta_{1Nf})$ in (28) is obtained as $(0, \pi)$, which further satisfies the relation provided in (29).

$$sin(\theta_{1vf}^{upf} - \theta_{1Nf}) > 0 \tag{29}$$

$|S_1|$ obtained from (5) is always less than 1, as the magnitude of denominator is greater than the numerator. Similarly from (9), it is observed that $|S_1^{'}| < 1$ and the maximum value of $|S_1| + |S_1^{'}|$ is 1. Thus, $\left(\frac{|S_1^{'}|}{\sqrt{1+(P_3/P_1)^2}} + \frac{|S_1|}{\sqrt{1+(P_2/P_1)^2}}\right) \leq 1$. On the other side, fault current limit by PV inverter causes $|I_{1Sf}|$ to be significantly lower than $|I_{1Nf}|$. This results in $|I_{1Nf}|(1-x)sin(\theta_{1vf}^{upf} - \theta_{1Nf}) > |I_{1Sf}|$. With this consideration a relation is derived in (30).

$$|I_{1Nf}||(1-x)|sin(\theta_{1vf}^{upf} - \theta_{1Nf}) > |I_{1Sf}|P_4 \tag{30}$$

where, $P_4 = \left(\frac{|S_1^{'}|}{\sqrt{1+(P_3/P_1)^2}} + \frac{|S_1|}{\sqrt{1+(P_2/P_1)^2}}\right)$.

Applying the relation obtained from (30) in (26), a condition is established in (31) for faults in line-1.

$$\Delta Q_{1M} > 0 \tag{31}$$

Thus, it is evident from (23) and (31) that ΔQ_{1M} is positive for faults in line-1 and it is independent of PV plant operation mode. On the other hand, $I^{(1)}_{1Mf} = I^{(2)}_{2Mf}$ for normal operation and faults external to the parallel lines. This results in $Q^{(1)}_{1M} = Q^{(2)}_{1M}$, which is expressed as a condition provided in (32).

$$\Delta Q_{1M} = 0 \tag{32}$$

Thus, the conditions derived for correct operation of distance relays protecting parallel lines are as follows:

$$\begin{aligned} &\Delta Q_{1M} > Q_{1th}; \quad \text{for zone-1 fault in line-1} \\ &\Delta Q_{1M} < -Q_{1th}; \quad \text{for zone-1 fault in line-2} \end{aligned} \tag{33}$$

The threshold, Q_{1th} in (33) is decided considering a maximum 20% mismatch in $I^{(1)}_{1M}$ and $I^{(2)}_{2M}$ due to the measurement error during a bolted 3-phase fault at the relay bus [24]. However, the condition in (33) cannot be applied if any of the line is out of service for maintenance or any other reasons. Further, conventional distance relay at PV connected bus is also observed to maloperate at times during single circuit operation [25]. Therefore, a different check is required to derive correct protection decision for single circuit operation with such a line configuration in the system.

B. Identification of single circuit operating condition

Conditions of line-1 and line-2 are reflected through the status signal of both circuit breakers (CB_1 and CB_2). CB_1 and CB_2 will be at high state (1) when both the lines are in operation, whereas low output (0) at any of the breaker status indicates the respective line in out of service condition. Thus, the single circuit operation is identified in the system with parallel line configuration.

C. Protection method for single line operation

Distance relay at PV side is found to maloperate at times due to the limited and modulated fault current from the PV plant. Such an issue is not observed for the relay at the grid side. Thus, the influence of infeed current on PV-side distance relay operation can be avoided after successful opening of the breaker at the grid terminal. In such a condition the transmission line and the PV plant form a single infeed network and the impedance measured by the distance relay at PV side (Z_M) during a fault is expressed as

$$Z_M = \frac{V_{rM}}{I_{rM}} = xZ_{1L} + R_F. \tag{34}$$

Therefore, the distance relay configured on the PV side can operate correctly by incorporating a delay (T_d) into the protection logic coordinating with the fault clearing time at the grid end. This intentional delayed operation in the PV side relay is tolerable as the fault current is limited by the inverter. However, fault involving ground can result in high magnitude of current to flow in the line from the PV side due to the grounded path in the transformer connection. To mitigate such issue an additional zero sequence overcurrent check ($I_{OM} > I_{PU}$) is incorporated at the PV side.

D. Proposed scheme

An overview for implementing the proposed protection scheme is shown in Fig.6. For both lines in operation ($CB_1 = CB_2 = 1$), the line having higher positive sequence reactive power flow is identified as the faulted line to initiate tripping of the corresponding relay. A delayed distance relay operation is provided with zero sequence overcurrent check for proper protection during single line operation. For this the threshold (I_{PU}) of the zero sequence overcurrent relay is decided by the minimum ground current ($0.1I_{rated}$).

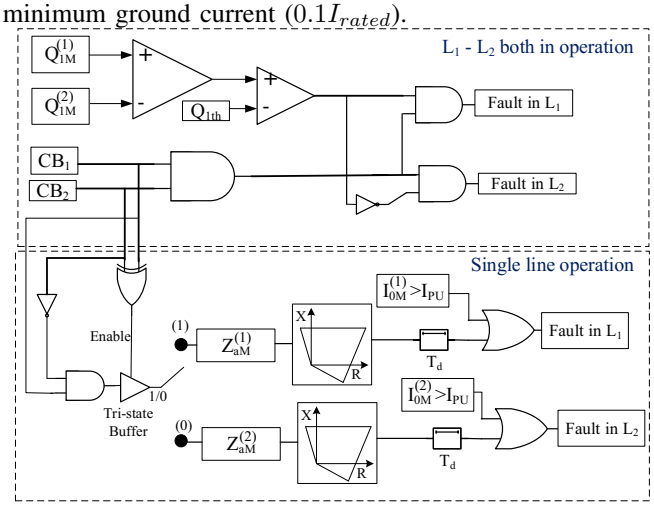

Fig. 6. Proposed protection scheme at the PV-side of the parallel lines.

V. RESULTS

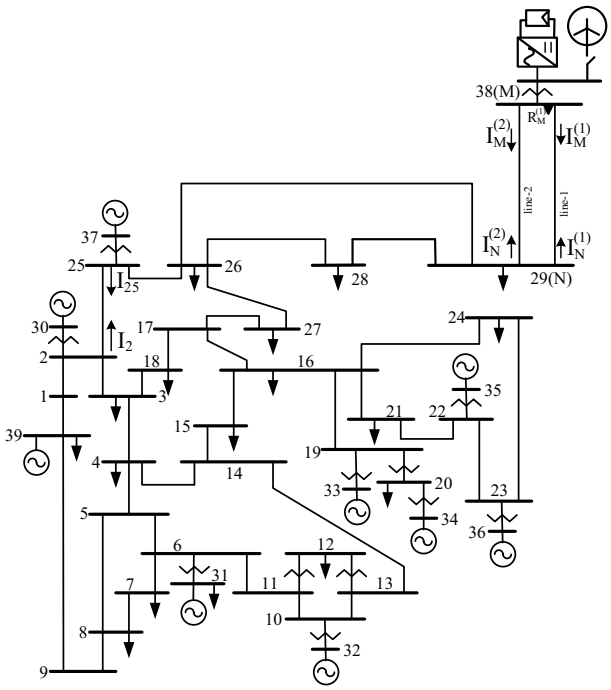

Fig. 7. New-England 39-bus integrated with PV plant.

The proposed method is tested for a 345 kV, 60 Hz, modified 39-bus New England system, as shown in Fig.7. The synchronous generator connected at bus 38 is replaced by a PV plant of capacity 300 MW, which is connected to bus 29 using a double circuit line. The PV plant is complied with different grid codes. In order to maintain the line flows similar to the standard system as in [26], loads at bus 28 and 29 are adjusted suitably. Simulations are carried out in PSCAD/EMTDC to generate different fault data. Performance of the proposed method is evaluated for the relay at bus 38 with the local end voltage and current (for both lines) measurements. Digital mimic filter is used to eliminate the decaying-DC component

of fault current. The measured data are sampled at a rate of 1.2 kHz. 1-cycle discrete Fourier transform (DFT) is applied to estimate voltage and current phasors, which are further processed to compute positive sequence components required for the proposed protection method. Comparative assessment with available approaches is provided to demonstrate the strength and high reliability of the proposed method. .

A. For different faults with variation in fault resistance

Limited fault current in the inverter associated with the solar plant results in significant magnitude difference between the phase currents at local and remote end of the faulted line. This difference is higher during the phase faults (BC and ABC) with low fault resistances. Similar situation arises during ground faults (BCG, AG) with significant fault resistance due to the reduction in zero sequence current from the PV side. Performance of conventional distance relay and the proposed method is tested for different faults created in line-1 connecting bus 38 and bus 29 in the 39-bus test system of Fig.7. Ground faults (AG and BCG) are created at a distance of 0.5 pu from bus 38 with a variation in $\mathrm{R_F}$ from 50 Ω to 100 Ω, whereas phase faults (BC and ABC) are created at 0.75 pu from bus 38 with a maximum $\mathrm{R_F}$ of 10 Ω. Performance of the distance relay $R_M^{(1)}$ (as shown in Fig.7) for the fault cases are provided in Table-I. Results demonstrate that the apparent impedance (Z_{app}^{M}) calculated by the relay deviates significantly from the actual faulted section impedance ($Z_{MF}^{act} = xZ_{1L}$) and remains outside the zone-1 in many cases (as indicated by shaded rows), even when the relay is set with a quadrilateral setting having a $\mathrm{R_F}$ coverage of 100 Ω [22].

TABLE I
PERFORMANCE OF CONVENTIONAL DISTANCE RELAY FOR DIFFERENT FAULT TYPES AND FAULT RESISTANCES

Fault type	R_F (Ω)	Z_{MF}^{act}		Z_{app}^{M}	
		R_{MF}^{act} (Ω)	X_{MF}^{act} (Ω)	R_{app}^{M} (Ω)	X_{app}^{M} (Ω)
ABC	1	3.85	56.25	19	58
	5	3.85	56.25	40	58.8
	10	3.85	56.25	75	64
BC	1	3.85	56.25	12	52
	5	3.85	56.25	25	59
	10	3.85	56.25	44	72
BCG	50	2.55	37.5	165	20.33
	75	2.55	37.5	243	18.37
	100	2.55	37.5	314	7.431
AG	50	2.55	37.5	65	43
	75	2.55	37.5	121	36.6
	100	2.55	37.5	125	50

Difference in positive sequence reactive powers in both lines (ΔQ_{1M}) is calculated at bus 38 for all the fault cases (as mentioned in Table-I) and shown in Fig. 8. It is observed that ΔQ_{1M} is above the set threshold (Q_{1th}) for all the cases. This confirms the improved performance of the proposed method compared to distance relay in identifying the Zone-1 faults in line-1 using the condition mentioned in (33).

B. For faults at different locations (internal and external)

Performance of the proposed method is tested for faults created at different locations, internal and external to the parallel lines connecting bus 38 and bus 29 in the 39-bus system of Fig.7. Phase-A-to-ground (AG) faults are created at different locations of line-1 and line-2 with $\mathrm{R_F} = 10\ \Omega$. Fault location in both lines is varied form 0.1 to 0.9 pu (from bus 38). A 3-phase fault is created in line 26-29 with R_F = 0.1Ω, at a distance of 0.1 pu from bus 29 to present a forward external fault for the relay at bus 38. Similarly, a reverse fault case is presented by creating a 3-phase fault between bus 38 and the transformer connecting PV plant (with R_F = 0.1Ω). Positive sequence reactive power differences (ΔQ_{1M}) calculated for all the cases at bus 38 are shown in Fig.9 (a). It is evident that ΔQ_{1M} is greater than the threshold (Q_{1th}) for faults in line-1, whereas ΔQ_{1M} is negative and lower than the threshold ($-Q_{1th}$) for faults in line-2. ΔQ_{1M} obtains a value within the thresholds for both external faults. Results clearly demonstrate the correct operation of the proposed method for all internal and external fault cases using the conditions in (33).

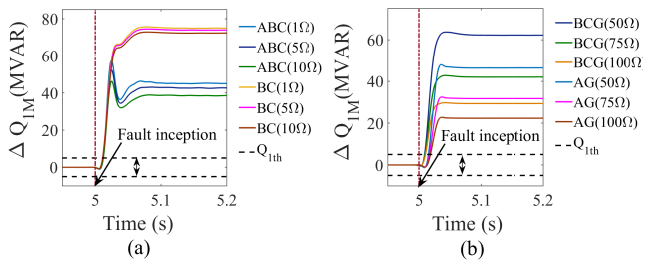

Fig. 8. Performance of the proposed method for (a) phase faults (ABC, BC) and (b) ground faults (AG,BCG) in line-1 with different fault resistances.

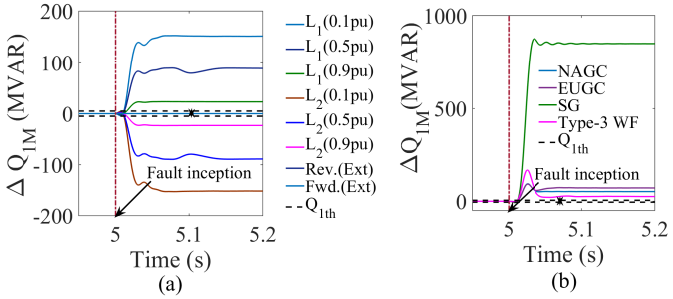

Fig. 9. Performance of the proposed method for faults (a) at different locations and, (b) with different sources complying different grid codes.

C. In the presence of different sources with different grid codes

Voltage and current during faults are modulated differently with variation in control operation associated with different sources and grid codes. Performance of the proposed method is tested in both the conditions for 3-phase faults created in line-1 connecting bus 38 and 29 in the 39-bus system, at a distance of 0.5 pu from bus 38 with $R_F = 0.1\Omega$. For the purpose, the PV plant connected at bus 38 is complied with the grid codes mentioned in [20] and [25], one at a time. The PV plant operates in upf mode (NAGC) while complied with the grid code in [20], whereas the plant supplies dynamic reactive current during fault when it is complied with the grid code in [25] (EUGC). In order to verify the compatibility of the proposed method with different sources, the method is tested with a 300 MW Type-III wind farm (replacing the PV plant) and a synchronous generator (as present in actual system in [26]) connected at bus 38, one at time. ΔQ_{1M}

calculated at bus 38 is found positive and higher than Q_{1th} for all the cases, as shown in Fig.9 (b). This clearly indicates correct identification of Zone-1 faults in line-1 and establishes the proposed protection method to be independent of control schemes associated with different sources and grid codes.

D. Performance of the proposed method for cross country fault

Performance of the proposed method is now tested for a cross-country fault in double circuit lines sharing the same tower. For this purpose, an AG fault is created in line-1 connecting bus 38 and bus 29 in Fig.7, at a distance of 0.4 pu from bus 38 with R_F = 20 Ω. At the same instant, a BG fault is created in line-2, at a distance of 0.5 pu from bus 38 with R_F = 25 Ω. ΔQ_{1M} computed at bus 38 is found higher than Q_{1th} (as shown in Fig.10 (a)), which initiates the tripping of circuit breaker only in line-1. Opening of circuit breaker in line-1 changes the parallel line configuration to single circuit operation mode. Now, the fault in line-2 is taken care by the protection arrangement present in the proposed scheme for single circuit operation comprising of delayed distance relaying and zero sequence overcurrent check. Result in Fig.10 (b) shows the zero-sequence current in line-2 ($I_{0M}^{(2)}$) to be higher than the pickup setting (I_{PU}). This demonstrates the correct operation of the proposed protection method for cross-country faults in parallel lines. In addition, the case study also verifies the performance of the proposed method during single circuit operation.

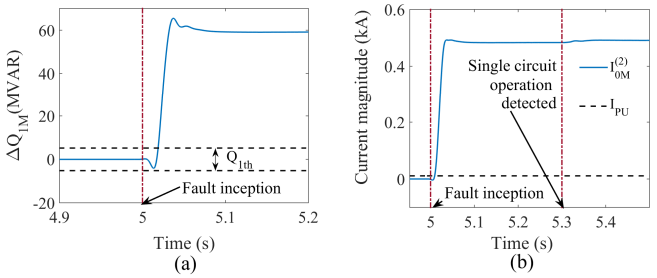

Fig. 10. Performance of the proposed method for a cross-country fault in parallel lines showing (a) ΔQ_{1M} and (b) $I_{0M}^{(2)}$.

E. Performance evaluation in the presence of interharmonics

Interharmonics present in a system with power-electronic converter based sources create issues for phasor estimation and influence the performance of associated protection schemes. Therefore, the performance of the proposed non-unit protection technique is tested in the presence of interharmonics. For this purpose, the current signals measured at bus 38 of Fig.7 (solar plant connected bus) is contaminated with the dominant interharmonics ranges from 32.5 Hz - 67.5 Hz considering the sampling frequency of MPPT algorithm and the fundamental frequency to be 10 Hz and 60 Hz respectively [27]. Further, a BC fault is created in line-1 connecting bus 38 and bus 29 in the 39-bus system, at a distance of 0.8 pu from bus 38 with R_F = 0.1Ω. The frequency spectrum of line -1 currents during prefault and fault conditions are shown in Fig.11 (a) and (b), with the current waveform in Fig.11(c). Higher value of ΔQ_{1M} than Q_{1th} (as shown in Fg.11(d)) indicates the fault to be in Zone-1 of line-1, and demonstrates the correct performance of the proposed method even in the presence of interharmonics.

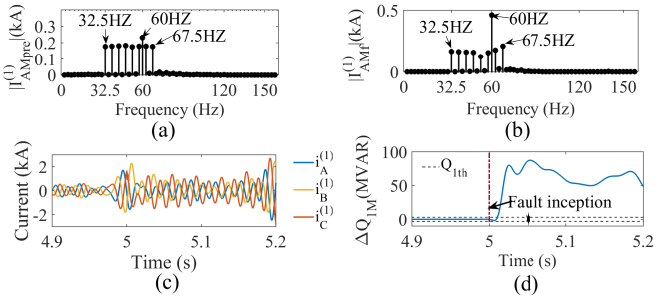

Fig. 11. Performance evaluation in the presence of inter-harmonics showing frequency spectrum of line-1 during (a) prefault, and (b) fault, with (c) inter-harmonic contaminated current signal and (d) ΔQ_{1M} calculated at bus 38.

F. Performance of the proposed method during power swing

Significant reduction in system inertia with integration of converter-interfaced sources may cause severe oscillations (like power swing) following a disturbance in the system. Performance of the proposed method is tested for fault during such an event. A 300 MW Type-III wind farm is connected at bus 38 of Fig.7, replacing the PV plant and sharing the total generation of the synchronous generator present in the actual system available in [26]. A three phase fault is created in line 26-29 at 7.3s, which is cleared by opening the circuit breakers at both ends of the line at 7.35s. As a result, a power swing is observed in the system. An AG fault is created in line-2 connecting bus 38 and 29 at 8.5 s with R_F = 10 Ω. Fig.12(a) and (b) show the voltages at bus 38 and currents in line-2 respectively. ΔQ_{1M} calculated at bus 38 is shown in Fig.12 (c). It is observed that ΔQ_{1M} remains within the threshold ($\pm Q_{1th}$) during prefault and crosses it only after the fault inception. ΔQ_{1M} lower than $-Q_{1th}$, as shown in Fig.12(c), indicates correct identification of Zone-1 fault in line-2 using the proposed method even during the power swing.

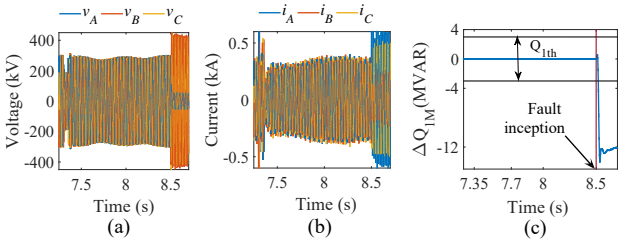

Fig. 12. Performance of proposed method for fault during power swing showing (a) voltage at the relay bus (b) current in the faulted line, and (c) the positive sequence reactive power difference

G. Performance of the proposed method in an Indian power network for different power flow conditions

The performance of the proposed method is tested for different power flow conditions by simulating a part of the Indian power grid with parallel lines connecting PV plant to the grid, as shown in Fig.13. Detail system parameters as in [1] are provided in Appendix-II and the load connected at bus M is considered to be 400 MW. For this purpose phase-A-to-phase-C (AC) faults are created in line-1 at a distance of 0.5

pu from bus M (Kasorgode S/S) of Fig.13 with $R_F = 0.1\ \Omega$. The solar plant generation is varied from 125 to 500 MW. PV plant generation less than 400 MW indicates the power flow to be from bus N to bus M. Positive sequence reactive power difference calculated at bus M and N (ΔQ_{1M} and ΔQ_{1N}) are shown in Fig.14. Higher values of ΔQ_{1M} and ΔQ_{1N} than Q_{1th} for all the cases ensure correct identification of Zone-1 faults in line -1 using the proposed method. This also verifies the method to be independent of power flow conditions.

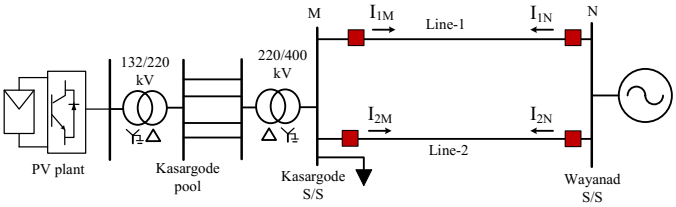

Fig. 13. Transmission system for Kasargode solar park in Kerala [1].

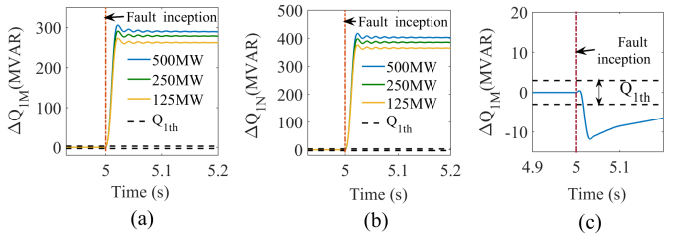

Fig. 14. Performance of the proposed method for relay installed at (a) bus M and (b) bus N of Fig.13 for line-1 faults with varying solar plant capacity, and (c) bus M in Fig.15 for line-2 fault

H. Performance of the proposed method for a system with 100% PV penetration

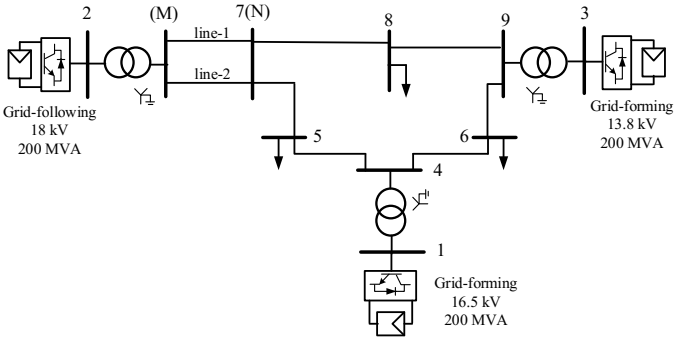

Fig. 15. 9-bus system with 100% PV penetration.

Performance of the proposed method is tested for a 9-bus system with 100% PV penetration, as shown in Fig.15 [28]. The solar plant connected at bus 2 is integrated to the grid through grid-following converter, whereas the solar plants at bus 1 and 3 are integrated through grid-forming converters. The grid-following converter operates with balanced current controller, whereas the grid-forming converters are controlled with dual-current controller and generate both positive and negative sequence currents. An AG fault is created in line-2 (as marked in the system) at a distance of 0.7 pu from bus M with R_F = 20Ω. The reactive power difference (ΔQ_{1M}) calculated by the proposed method at bus M is found to be less than the threshold (Q_{1th}) (as shown in Fig.14(c)), which indicates the correct identification of zone-1 fault in line-2. Thus, the proposed method is found to be robust even for the system with 100% PV penetration.

I. Comparative assessment

Limitations of the available methods (as mentioned in Section I) are summarized in Table II and compared with the proposed method. In order to present the high reliability of the proposed method with quantitative measure, the method is tested for total 1920 fault scenarios as listed in Table III. Fault resistance is varied from 0.1Ω to 100Ω for ground faults, whereas it is varied up to 30Ω for ungrounded faults. Conventional distance protection and cross-differential relaying techniques are also tested for those cases. The distance relay reach has been increased to 90% to provide a uniform comparative assessment. The formula available in [29] is applied to calculate the reliability of the protection methods. The study reveals the reliability of distance relay and cross-differential technique to be 65% and 85% respectively, whereas the proposed method is found to be 100% reliable, providing correct results for all cases. Some of those cases are provided below highlighting the comparative assessment.

TABLE II
COMPARATIVE ASSESSMENT WITH AVAILABLE METHODS

Parameters	Available Methods				Proposed Method
	[5]–[7]	[12], [13]	[14], [16]	[17]	
Applicable to parallel lines?	Yes	Yes	No	Yes	Yes
Tested for renewable integrated system?	No	No	Yes	No	Yes
Independent of source control algorithms?	No	No	Yes	No	Yes
Insensitive to mutual impedance?	No	No	No	No	Yes
No requirement of faulted phase selection?	No	No	No	No	Yes

TABLE III
LIST OF FAULT CASES FOR COMPARATIVE ASSESSMENT

Fault types	AG,BG,CG,AB,BC,CA,ABG,BCG,CAG,ABC
Fault resistance(Ω)	0.1, 10, 30, 50, 75, 100
Fault locations (pu)	0.1, 0.25, 0.75, 0.9, 1
Grid Code	NAGC, EUGC
PV plant capacity (%)	25, 50, 75, 100
Total cases = (6x6x5x2x4)+(4x3x5x2x4)=1920	

1) For different fault types with variation in fault resistance and fault location: Fig.16 presents the comparative assessment between cross differential relaying and the proposed method for different types of faults (with R_F = 0.1 Ω) created in the line-1 connecting bus 38 and 29 in the 39-bus test system with variation in fault location and PV plant generation capacity. The solar plant is considered to operate in upf mode following NAGC. As shown in Fig.16(a), the cross-differential method is found to maloperate for ungrounded faults. This is due to the severe fault current modulation by the solar plant in the absence of zero sequence current. On the other hand, the proposed method is found to operate correctly for all the fault cases, as shown in Fig.16(b).

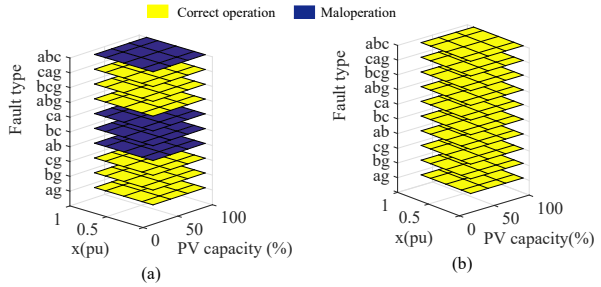

Fig. 16. Performance of (a) cross-differential, and (b) the proposed method for different fault types with variation in fault location and PV plant capacity.

2) For different PV capacities with variation in fault location and fault resistance: A similar comparative assessment between distance relaying and the proposed method is provided in Fig.17 for BCG faults created in line-1 connecting bus 38 and 29 in the 39-bus system with variation in fault resistance, fault location and PV generation capacity. Similar to the earlier case, the solar plant is considered to operate in upf mode following NAGC. As shown in Fig.17(a), the distance relay is found to maloperate for faults near to the relay reach with significant fault resistance. It is also observed that the chance of relay maloperation increases with reduction in solar plant generation. This is due to the increase in local end source impedance. On the other hand, the proposed method is found to operate correctly for all the fault cases generated for this study, as shown in Fig.17(b).

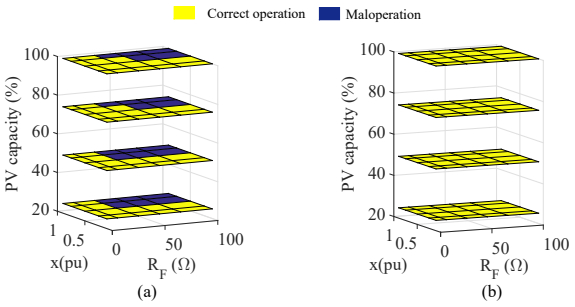

Fig. 17. Performance of (a) conventional distance relay and (b) the proposed method for BCG faults with variation in fault resistance, fault location and PV plant capacity.

VI. Conclusion

Techniques available for parallel line protection are not reliable while connected to solar PV plant. A method is proposed to identify Zone-1 faults in parallel lines using the positive sequence reactive power difference between both the lines. A delayed distance protection with additional ground current checking is included in the protection logic at the PV side for single circuit operation. The method uses only local voltage and current data for protecting the parallel lines. The performance of the proposed method is tested for different types of faults with variation in fault resistance, location, power flow condition and PV penetration level. The applicability of the proposed method is demonstrated for lines connecting other renewable sources and with different grid code compliances. The performance is also tested for cross-country faults, in the presence of inter-harmonics and during power swing. Comparative assessment with the available techniques demonstrates the strength and high reliability of the proposed method.

Appendix -I

A. Calculation of θ_{1vf}

From Fig. 3 the positive sequence voltage V_{1Mf} observed at bus M during BCG fault in line-1 is given by

$$V_{1Mf} = I^{(1)}_{1Mf}(xZ_{1L}) + Z_F(I^{(1)}_{1Mf} + I^{(1)}_{1Nf}) \tag{35}$$

and the positive sequence current $I^{(1)}_{1Nf}$ can be obtained from

$$I^{(1)}_{1Nf} = I_{1Nf}\frac{(1+x)}{2} + I_{1Sf}\frac{xZ_{1G}-Z_F}{Z_{1L}(1-x^2)+2Z_{1G}+2Z_F} \tag{36}$$

After replacing the value of $I^{(1)}_{1Mf}$ and $I^{(1)}_{1Nf}$ from (4) and (36) in (35), V_{1Mf} can be simplified as

$$V_{1Mf} = [I_{1Sf}Z_{1L}D_1 + E_{1Gf}K_1] \tag{37}$$

Considering the transmission line resistance to be negligible, θ_{1vf} with respect to the grid side voltage E_{1Gf} is obtained from

$$\theta_{1vf} = sin^{-1}[\frac{|I_{1Sf}||X_{1L}||D_1|cos(\angle D_1 - \theta_f)}{|E_{1Gf}||K_1|}] + \angle K_1 \tag{38}$$

The value of D_1 and K_1 are expressed as

$$D_1 = \frac{x(1-x)Z_{1L} + x(2-x)Z_{1G} + Z_F}{Z_{1L}(1-x^2) + 2Z_{1G} + 2Z_F}$$
$$K_1 = \frac{x(1-x)Z_{1L} + 2Z_F}{Z_{1L}(1-x^2) + 2Z_{1G} + 2Z_F} \tag{39}$$

Appendix -II

B. System Parameters

TABLE IV
Simulation Parameters of the System in Fig. 1

Element	Parameter	Value
PV plant	Unit Capacity	1MW
	Total no of units	300
Transformer	Voltage level, Frequency	33/230kV, 60Hz
	Vector group	YNd11
	MVA, %Z	400, 7%
PI controller	Current controller (d-q axis)	K_p=0.15 T_i=0.08s
DC bus	Rated Voltage DC link capacitor	600V 7800μF
Filter	L_f, C_f, R_f	300μH,200μF 25$m\Omega$
Transmission line	Voltage, Line length	230kV, 150km
	Line Model	Tower type, 3L12
	Conductor type	Chuckar
CT	Ratio, Class Core	1000:1, 5P40, Silectron 53
PT	Ratio, Class	400kV:110V, 3P

TABLE V
SIMULATION PARAMETERS FOR THE INDIAN SYSTEM OF FIG. 13

Transmission Line	Voltage Level: 400 kV
	Length: 220 km
	Transmission line model: Tower type, 3L14
	Transmission line conductor: Moose
Solar plant	Rated capacity: 500 MW
Transformer	700 MVA, 220 kV/ 400 kV, YNd1

REFERENCES

[1] Green energy corridors II (Part-A): A plan for integration of ultra mega solar power parks, Power Grid Corporation of India Ltd. [Online]. Available: https://www.powergridindia.com/sites/default/files/Our Business/Smart-Grid/2017/1/Green/20Energy/20Corridor/202-Part20A.pdf.

[2] H. Lund and B. V. Mathiesen, "Energy system analysis of 100% renewable energy systemsthe case of denmark in years 2030 and 2050," *Energy*, vol. 34, no. 5, pp. 524–531, 2009.

[3] Y. Wang and B. Ren, "Fault ride-through enhancement for grid-tied PV systems with robust control," *IEEE Trans. Indus. Electr.*, vol. 65, no. 3, pp. 2302–2312, March 2018.

[4] A. Apostolov, D. Tholomier, S. Sambasivan, and S. Richards, "Protection of double circuit transmission lines," *Proc.* 60^{th} *Annu. Conf. Protective Relay Eng.*, pp. 1–17, Mar 2007.

[5] H. Teimourzadeh, B. M. Ivatloo, and M. Shahidehpour,"Adaptive protection of partially coupled transmission lines" *IEEE Trans. Power Del.*, vol. 36, no. 1, pp. 429–440, Feb 2021.

[6] V. Ashok, and A. Yadav,"Fault diagnosis scheme for cross-country faults in dual-circuit line with emphasis on high-impedance fault syndrome" *IEEE Syst. J.*, vol. 15, no. 2, pp. 2087–2097, June 2021.

[7] K. Jia, T. Bi, Y. Fang, W. Li, and Q. Yang, "Ground fault distance protection for paralleled transmission lines" *IEEE Trans. Indus. Appl.*, vol. 51, no. 6, pp. 5228–5236, Nov/Dec 2015.

[8] B. R Bhalja, R. P. Maheshwari "High-resistance faults on two terminal parallel transmission line: analysis, simulation studies, and an adaptive distance relaying scheme," *IEEE Trans. Power Del.*, vol. 22, no. 2, pp. 801–812, April 2007.

[9] Y. Hu, D. Novosel, M. M. Saha, and V. Leitloff,"An adaptive scheme for parallel-line distance protection," *IEEE Trans. Power Del.*, vol. 17, no. 2, pp. 105–110, Jan 2002.

[10] O. A Gashteroodkhani, M. Majidi, and M. A. Amoli "A fault data based method for zero-sequence impedance estimation of mutually coupled transmission lines," *IEEE Trans. Power Del.*, vol. 36, no. 5, pp. 2768–2776, Oct 2021.

[11] S. H. Horowitz, A. G. Phadke, Power system relaying. John Wiley and Sons, 2008. (pp.-133-151)

[12] S. Li, W. Chen, X. Yin, D. Chen and O. P. Malik "Integrated transverse differential protection scheme for double-circuit lines on the same tower,," *IEEE Trans. Power Del.*, vol. 33, no. 5, pp. 2161–2169, Oct 2018.

[13] M. S Pasand, and P. Jafarian "Adaptive protection of parallel transmission lines using combined cross-differential and impedance-based techniques," *IEEE Trans. Power Del.*, vol. 26, no. 3, pp. 1829–1840, July 2011.

[14] S. Paladhi and A. K. Pradhan, "Adaptive distance protection for lines connecting converter-interfaced renewable plants," *IEEE J. Emerg. Sel. Topics Power Electr.*,vol. 9, no. 6, pp.7088–7098, Dec 2021.

[15] A. Banaiemoqadam, A. Hooshyar, and M. A. Azzouz, "A control-based solution for distance protection of lines connected to converter-interfaced sources during asymmetrical Faults," *IEEE Trans. Power Del.*, vol. 35, no. 20, pp. 1455–1466, June 2020.

[16] Y. Fang, K. Jia, Z. Yang, Y. Li, and T. Bi, "Impact of inverter-interfaced renewable energy generators on distance protection and an improved scheme," *IEEE Trans. Indus. Electr.*, vol. 66, no. 9, pp.7078–7088, Sept 2019.

[17] W. Zhou, F. Li, C. Xie, B. Wang,L. Gong and S. Yang "Adaptive autoreclosing scheme for line-to-line nongrounded faults on double-circuit transmission lines based on phase-to-phase reactive Power," *IEEE Access*, vol. 8, pp. 144092–144104, Aug 2020.

[18] S. V Unde, P. Gawande and S. Dhambhare "New algorithm for protection of double circuit transmission lines using modal currents," *IEEE Trans. Power Del.*, vol. 34, no. 5, pp. 1967–1977, Oct 2019.

[19] S. Paladhi and A. K. Pradhan, "Adaptive fault type classification for transmission network connecting converter-interfaced renewable plants," *IEEE Syst. J.*, vol. 15, no. 3, pp. 4025–4036, Sept 2021.

[20] "Reliability guideline: BPS-connected inverter-based resource performance," North American Electric Reliability Corporation, Atlanta, GA, Tech. Rep., September 2018.

[21] A. Chowdhury, S. Paladhi, and A. K. Pradhan "Adaptive unit protection for lines connecting large solar plants using incremental current ratio" *IEEE Syst. J.*, vol. 16, no. 2, pp. 3272–3283, June 2022.

[22] "Line Distance Protection REL670," May 2017, ABB application manual.

[23] M. A. Azzouz, A. Hooshyar and E. F. El-Saadany, "Resilience enhancement of microgrids with inverter-interfaced DGs by enabling faulty phase selection,," *IEEE Trans. Smart Grid*, vol. 9, no. 6, pp. 6578–6589, Nov. 2018.

[24] A. H. Osman, and O. P. Malik, "Protection of parallel transmission lines using wavelet transform," *IEEE Trans. Power Del.*, vol. 19, no. 1, pp. 49–55, Jan 2004.

[25] A. Hooshyar, M. A. Azzouz, and E. F. El-Saadany, "Distance protection of lines emanating from full-scale converter-interfaced renewable energy power plants, Part I: Problem statement," *IEEE Trans. Power Del.*, vol. 30, no. 4, pp. 1770–1780, Aug 2015.

[26] I. Hiskens "IEEE PES task force on benchmark systems for stability controls," Tech. Rep., Nov. 2013 [Online]. Available: http://eioc.pnnl.gov/benchmark/ieeess/IEEE39/New England Reduced Model (39 bus system) MATLAB study report.pdf

[27] A. Sangwongwanich, Y. Yang, D. Sera, H. Soltani , and F. Blaabjerg "Analysis and modeling of interharmonics from grid-connected photovoltaic systems" *IEEE Trans. Power Electron.*, vol. 33, no. 10, pp. 8353–8364, Oct 2018.

[28] A. Zitouni "Open-source PSCAD grid-following and grid-forming inverters and a benchmark for zero-inertia power system simulations,," *IEEE Kansas Power and Energy Conference (KPEC)*, pp. 1–6, 2021.

[29] A. Zitouni "Power transformer differential relay reliability assessment using false trip root cause analysis.," *Int. Conf. Electr. Eng. (ICEE)*, Sept. 25–27, 2020.